Cell Reports, Volume *27*

Supplemental Information

PCNA-Mediated Degradation of p21 Coordinates the DNA Damage Response and Cell Cycle Regulation in Individual Cells

Caibin Sheng, Isabella-Hilda Mendler, Sara Rieke, Petra Snyder, Marcel Jentsch, Dhana Friedrich, Barbara Drossel, and Alexander Loewer

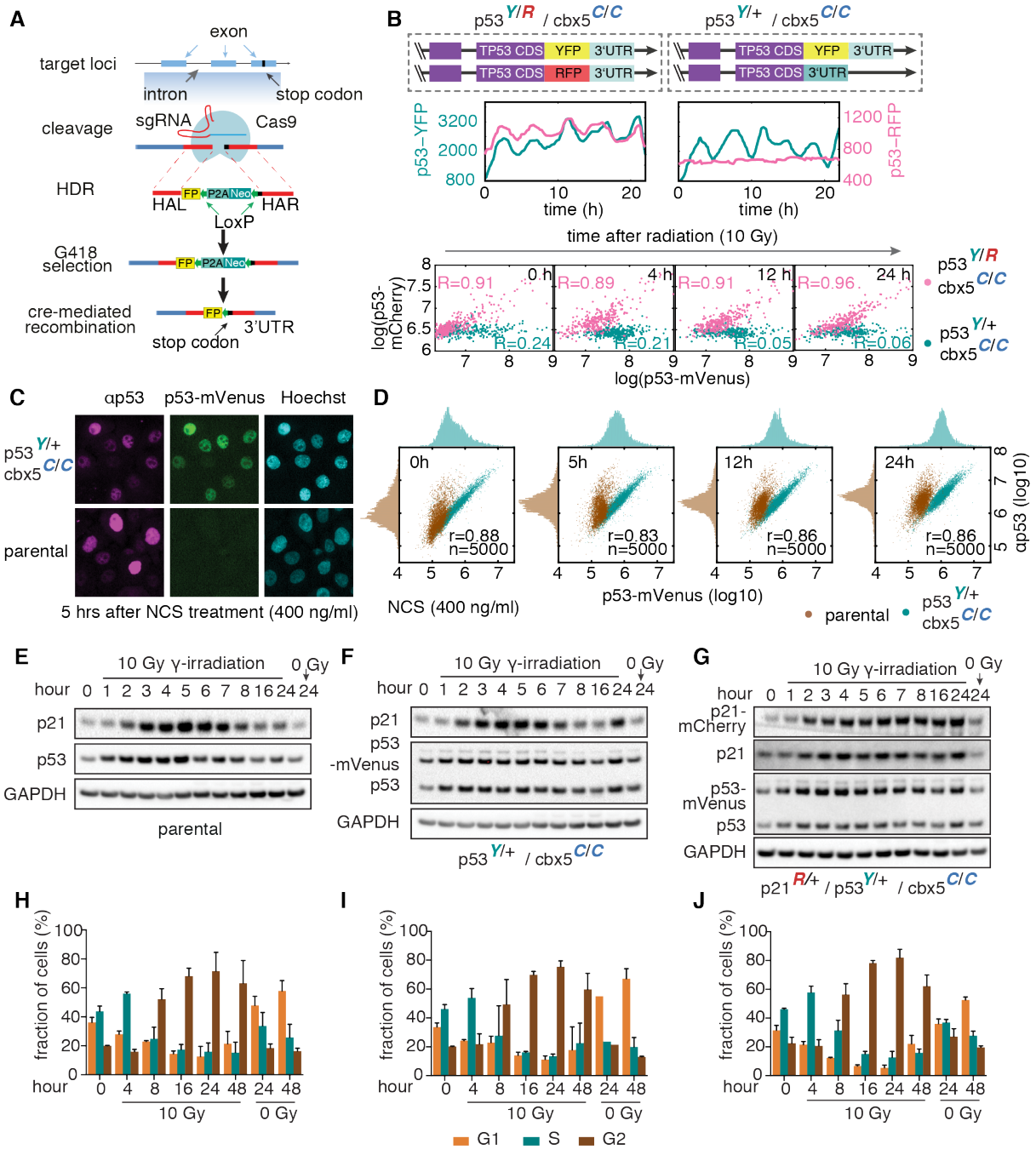

Figure S1. Endogenous tagging of p53 and p21 allows to faithfully monitor protein levels, related to Figure 1A

(A) CRISPR/Cas9-mediated engineering allows insertion of fluorescent genes in endogenous loci. FP - fluorescent protein, P2A - self-cleavage peptide, Neo – G418/neomycin resistance, LoxP - LoxP sequence for Cre-mediated recombination, HDR – homology dependent repair. A SEPT cassette was used instead of P2A-Neo for some repair templates (see STAR methods).

(B) A heterozygous fluorescent protein tag is sufficient for monitoring endogenous p53 level. Both alleles of p53 were tagged with mVenus (YFP) and mCherry (RFP), respectively, to visualize allele-specific p53 expression. 3'UTR represent the untranslated 3'-region; YFP, RFP and CFP indicate mVenus, mCherry and Cerulean. Cbx5 encodes Chromobox Protein Homolog 5, regarded as a nuclear marker. Cells were treated with 10Gy γ-irradiation and followed by time-lapse microscopy for 24 h. Examples for allele-specific p53 expression ($p53^{Y/R}$ / $cbx5^{C/C}$) and control cells with a single tagged p53 ($p53^{Y/+}$/ $cbx5^{C/C}$) allele are shown. The correlation of protein levels expressed from both alleles is shown at indicated time points. R-values represent Pearson correlation coefficients from randomly sampled cells (n=300 for each line).

(C, D) Single cell immunofluorescence staining validates endogenous fluorescent reporter. Wild type MCF10A and $p53^{Y/+}$/ $cbx5^{C/C}$ cells were treated with the radiomimetic drug NCS (400 ng/ml) and stained

with an antibody against p53 (C). 5000 cells were randomly sampled at selected time points and Spearman correlation coefficients (r) for $p53^{Y/+}$/ $cbx5^{C/C}$ cells are shown (D).
(E-G) Protein levels of p53 and p21 upon 10Gy ionizing radiation were evaluated at indicated time points by western blot in parental MCF10A cells (E), $p53^{Y/+}$/ $cbx5^{C/C}$ cells (F) and $p21^{R/+}$ / $p53^{Y/+}$ / $cbx5^{C/C}$ cells (G). GAPDH was used as a loading control.
(H-J) Cell cycle distributions upon 10Gy ionizing radiation were evaluated at selected time points by flow cytometry in parental MCF10A (H), $p53^{Y/+}$/ $cbx5^{C/C}$ cells (I) and $p21^{R/+}$ / $p53^{Y/+}$ / $cbx5^{C/C}$ cells (J). More than 10000 cells / per sample were analyzed. Three replicates were performed and mean with standard deviation is shown.

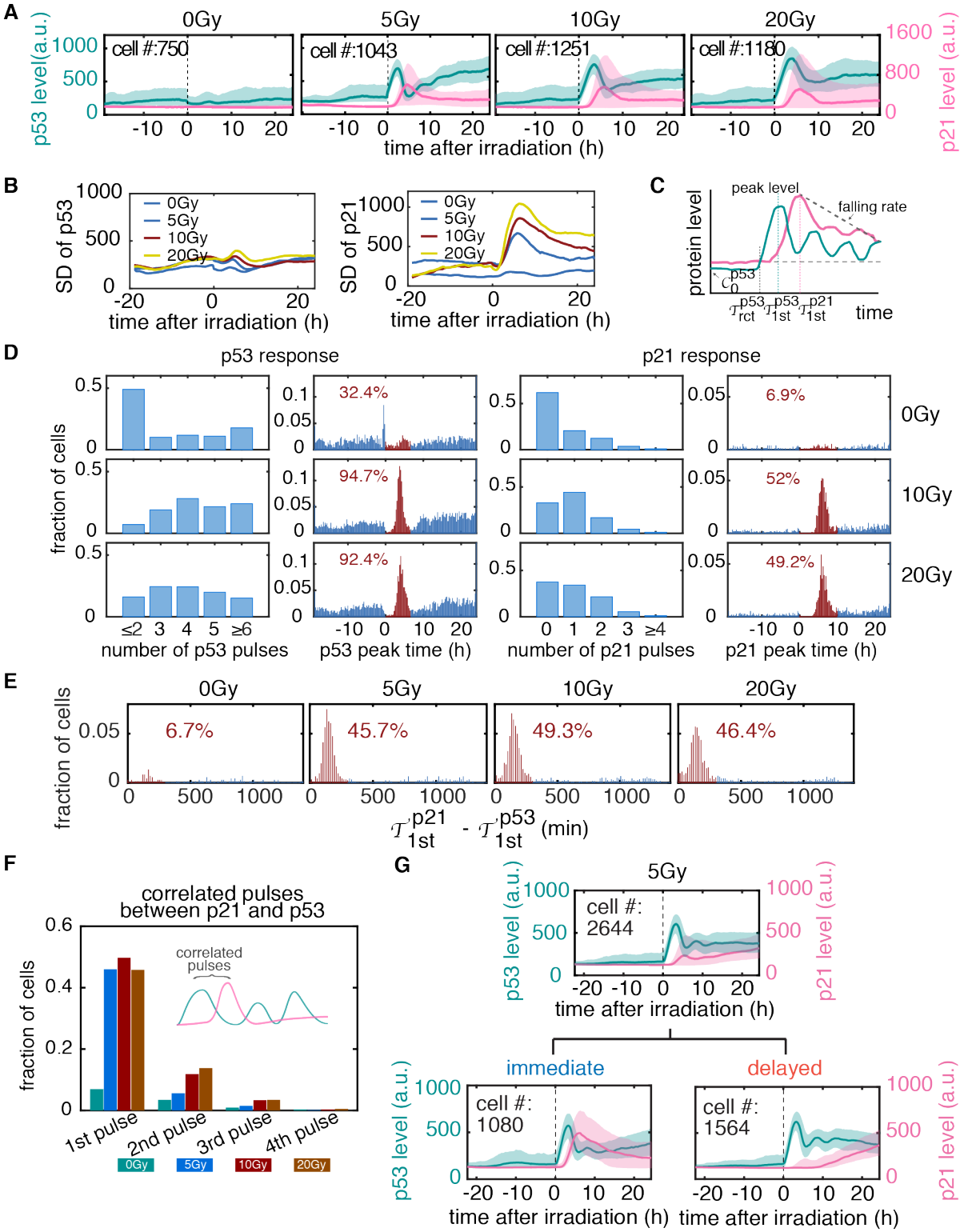

Figure S2. Heterogeneity of p21 responses is dose-independent in single cells, related to Figures 1B-F

(A, B) P21 dynamics diverge from p53 dynamics after various doses of ionizing radiation. The number of cells analyzed for each dose is indicated (see S2G for 5Gy). Lines indicate median protein levels, shaded areas the 25th to 75th percentile (green—p53; magenta—p21). Standard deviations of protein levels were calculated over time for p53 and p21 (B).

(C) Definition of dynamical features. T_{rct}, T_{1st}, and C_0 represents the timing of protein accumulation, timing of first peak and basal level, respectively. The superscripts indicate p53 and p21 proteins. See STAR methods for further details.

(D) Quantification of the number and timing of pulses shows similar responses in cell populations. Pulses occurring within 400 min (p53) and 600 min (p21) after irradiation are highlighted in red and the integrated fraction of cells is indicated. Cell numbers for each condition are indicated in (A).
(E) Delay between first p21 and p53 pulses. Delays within 300 min are highlighted in red and integrated fraction of cells is indicated. Cell numbers for each condition are indicated in (A).
(F) The fraction of cells with correlated p21 and p53 pulses. Correlated pulses are defined as p21 pulses occurring within 300 min after a p53 pulse. Cell numbers for each condition are indicated in (A).
(G) Population level of p53 and p21 in subgroups of cells. Two subgroups of first level by clustering are shown (related to Figures 1E and 1F).

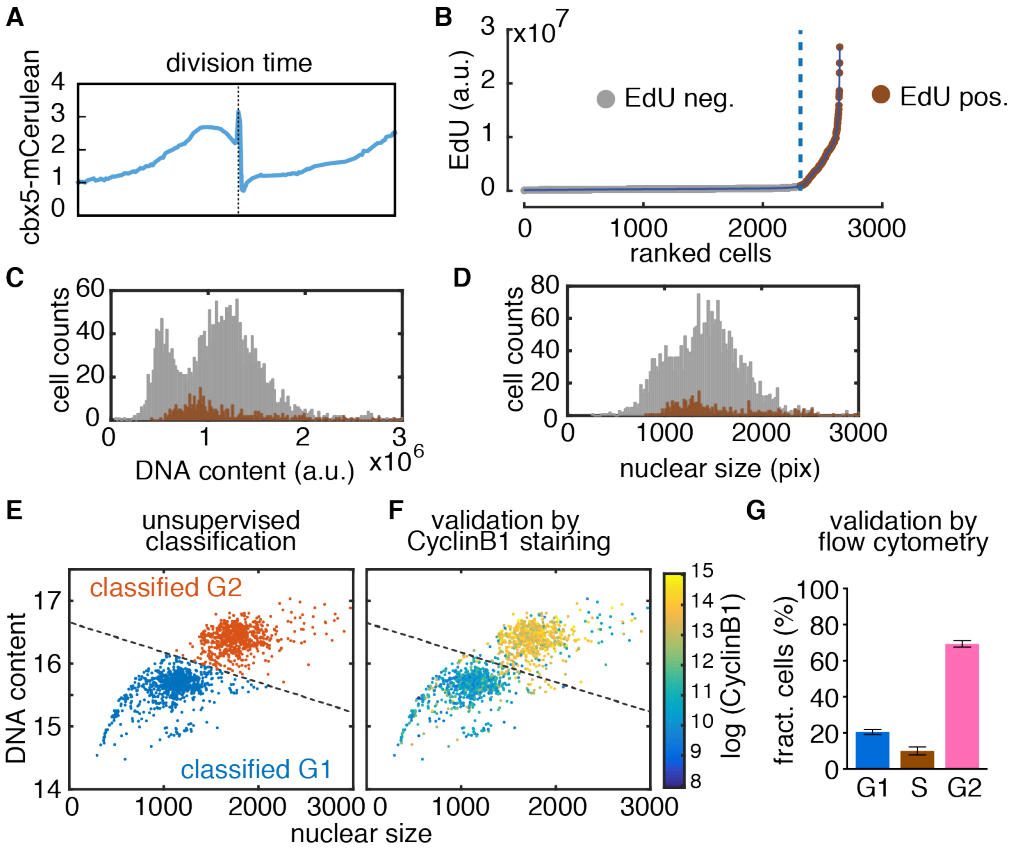

Figure S3. Cell cycle measurement for live-cell imaging, related to Figures 2A-C

(A) Intensity of the nuclear marker cbx5 over time. Bisection of nuclear marker levels indicate time of cell division, which was detected using a custom algorithm (dashed line, see STAR methods for further details).

(B) Identification of S-phase cells by EdU labeling. Cells were ranked by their EdU signals and a smooth line fitted to the distribution. EdU-positive cells were identified by an increased slope of the fitted function (dashed line, brown dots). n = 2644 cells.

(C, D) Histograms of DNA content (C) and nuclear size (D). Nuclei were stained with Hoechst, brown bars represent EdU positive cells (S-phase) as shown in B, gray bars represent EdU negative cells (G1- and G2-phase). Neither DNA content (C) nor nuclear size (D) individually enables distinction of G1- and G2-phase cells.

(E) Identification of G1- and G2-phase cells by a two parameter-based unsupervised classification. Blue and red dots represent estimated G1- and G2-phase cells, respectively. n = 1381 cells.

(F) Single cell immunofluorescence staining was performed to validate the classification in (E). CyclinB1 was quantified as indicators of G1- and G2-phase. CyclinB1 level is scaled from blue ($CyclinB1^{low}$) to yellow ($CyclinB1^{high}$).

(G) Cell cycle analysis by flow cytometer shows similar cell cycle distribution compared with microscopy-based quantification (Figure 2C). The reporter cells were subjected to 5Gy irradiation, harvested at 24 hours, stained with PI and analyzed using flow cytometer. Three replicates were performed, with more than 10000 cells analyzed for each.

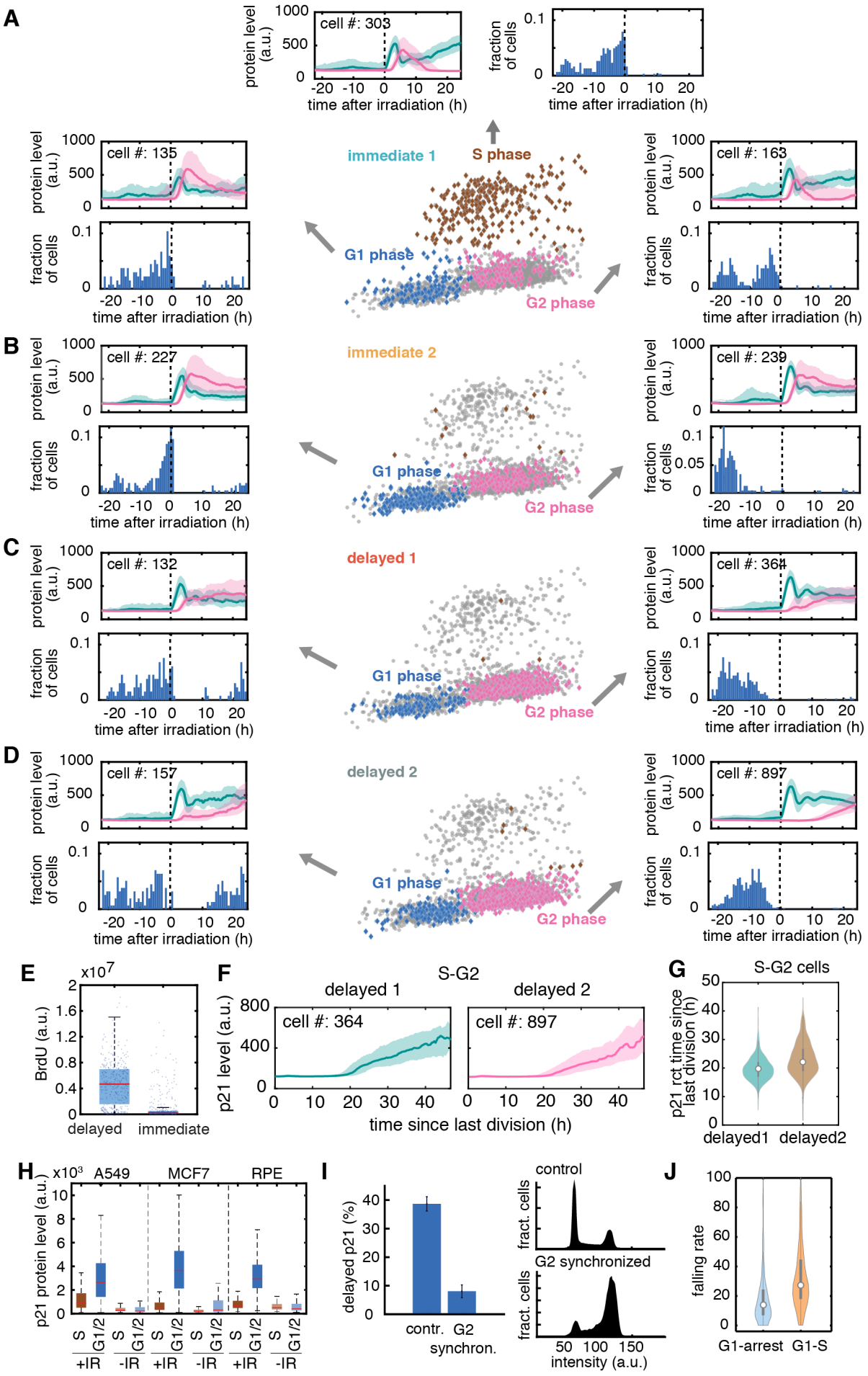
A
B
C
D
E
F
G
H
I
J
protein level (a.u.)
fraction of cells
time after irradiation (h)
cell #: 303
cell #: 135
cell #: 163
cell #: 227
cell #: 239
cell #: 132
cell #: 364
cell #: 157
cell #: 897
immediate 1
immediate 2
delayed 1
delayed 2
S phase
G1 phase
G2 phase
BrdU (a.u.)
delayed
immediate
S-G2
p21 level (a.u.)
time since last division (h)
S-G2 cells
p21 rct time since last division (h)
delayed1
delayed2
p21 protein level (a.u.)
A549
MCF7
RPE
+IR
-IR
delayed p21 (%)
contr.
synchron.
control
G2 synchronized
fract. cells
intensity (a.u.)
falling rate
G1-arrest
G1-S

Figure S4. Cells with varying dynamics showed different division time and final cell cycle stages, related to Figures 2D and 2E

(A) 'Immediate 1' cells tended to divide shortly before damage and ended in G1-phase (left), S-phase (up) or G2-phase (right). Final cell cycle phases for all cells are displayed (gray dots, bottom center), 'immediate 1' cells are highlighted using representative colors. Analysis of cell division time suggested that 'immediate 1' cells were mainly at G1-phase at the time of damage.

(B) 'Immediate 2' cells were arrested at G1-phase (left) or G2-phase (right).

(C, D) The majority of 'delayed' cells went through S-phase and arrested at G2-phase (right panels in C and D). Some 'delayed 1' cells were damaged and arrested at G1-phase (left in C). Cell cycle phase of the remaining cells were not determined as the division time distributed evenly before damage (left in D).

(E) Cells with 'delayed' and 'immediate' responses were validated as S-phase and G1/G2-phase cells, respectively. Cells were incubated with BrdU for 30 mins before damage and classified in a pool. 'Delayed' cells incorporated more BrdU than 'immediate' cells.

(F-G) The timing of p21 accumulation in S-G2 cells is correlated with last division before damage induction. *In silico* synchronization of cell cycle entry reveals that S-G2 cells within 'delayed 1' and 'delayed 2' accumulated p21 at similar time after division (F) but different time after damage induction (Figure 2D). Lines indicate median levels; shaded areas the 25th to 75th percentile (green—delayed 1; magenta—delayed 2). The number of S-G2 cells in each group is indicated. The duration between p21 accumulation and last division was calculated for each cell, resulting in similar distributions in 'delayed 1' and 'delayed 2' subgroups (G). White circles indicate median duration, bars indicate the 25th to 75th percentile, width of the shaded areas indicates the frequency.

(H) A549 (lung carcinoma), MCF7 (mammary carcinoma) and immortalized retinal pigment epithelia (RPE-hTERT) cells were pulse-labelled with EdU before irradiation with 5Gy. 6 h after damage induction, p21 levels were measured by immunofluorescence. In all cell lines, p21 levels were significantly lower in cells damaged in S-phase. Unirradiated cells are shown as comparison. Red lines indicate medians of distributions; boxes include data between the 25th and 75th percentiles; whiskers extend to maximum values within 1.5× the interquartile range (n>1000 cells/condition).

(I) P21 reporter cells were synchronized in G2 phase by treatment with the CDK1 inhibitor RO3306 for 16 h and irradiated with 5Gy. The p21 response was measured by live-cell microscopy. Fraction of cells with delayed p21 dynamics during the first 6 h were quantified in synchronized and control cells. Error bars represent standard error of the proportion. Synchronization was validated by flow cytometry (DNA content, upper and lower histogram).

(J) Quantification of p21 falling rate shows difference between G1-arrest and G1-S cells. n = 494 and 466 for G1-arrest and G1-S cells, respectively.

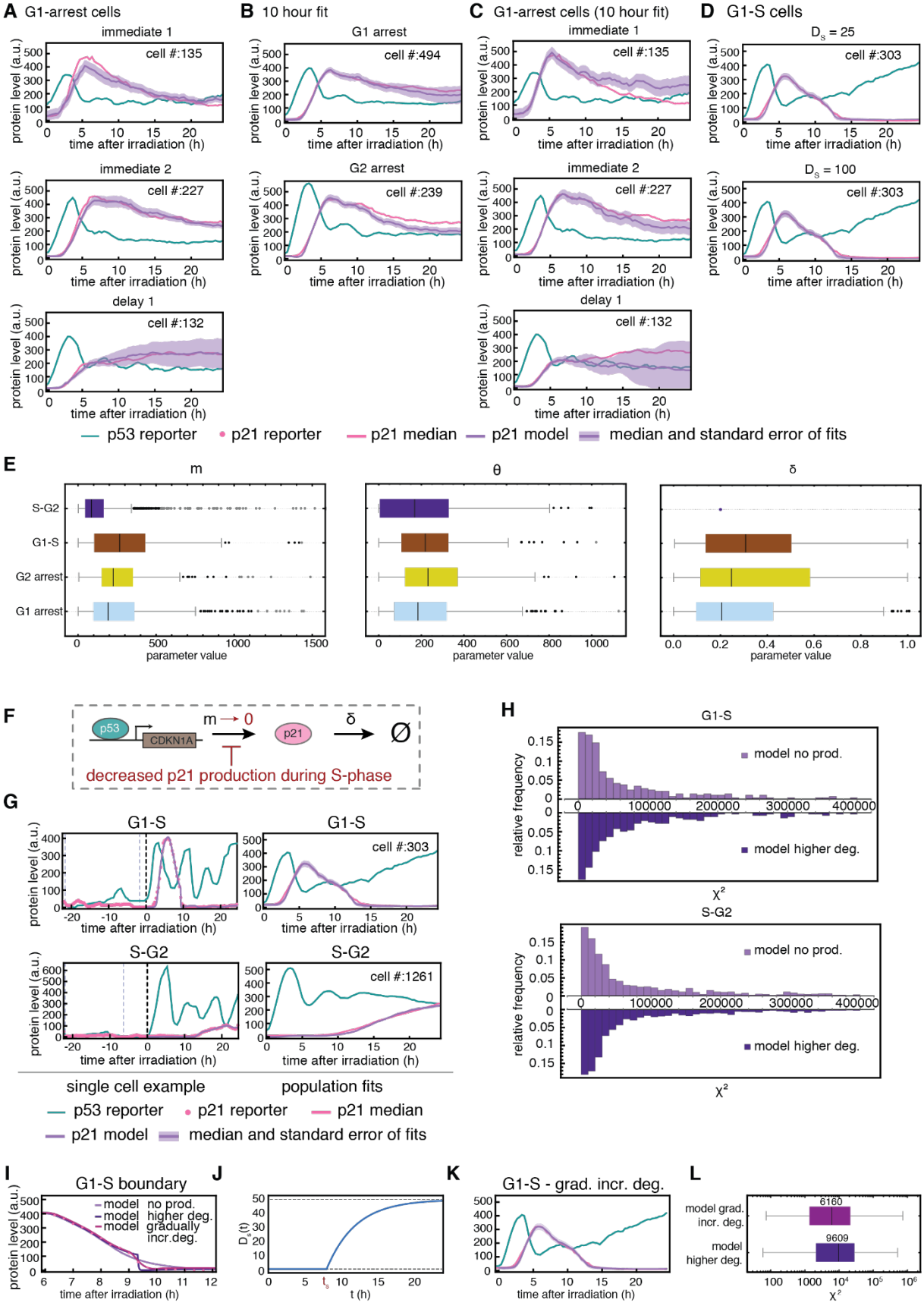

Figure S5. P21 dynamics in single cells and cell cycle specific subpopulations can be fitted by abstract mathematical models, related to Figure 3A-D

(A) Comparison of the simulation results (purple) and the median p21 levels (magenta) for the different subgroups of cells that arrested in G1. Shaded regions represent the standard error of the median. The

respective subgroup is indicated over the panels. The number of cells analyzed in each category is indicated.
(B) Comparison of the simulation results and the median p21 levels for all the cells that arrested either in G1 or G2, if the p21 concentration is only fitted until t=9.67 h. For each considered cell we performed a fit with 10 different randomly chosen initial values of the fit parameters and selected the best fit for averaging.
(C) Comparison of the simulation results and the median p21 levels for the different subgroups of cells that arrested in G1, if the p21 concentration is only fitted until t=9.67 h. For each considered cell we performed a fit with 10 different randomly chosen initial values of the fit parameters and selected the best fit for averaging.
(D) Comparison of the simulation results obtained for different values of D_S, i.e. different constant factors by which the degradation rate is multiplied during S phase, and the median p21 levels of multiple cells that were irradiated in G1 and progressed to S phase. The used values of D_S and the number of cells, for which the fits and the data were averaged, are indicated. Shaded regions represent the standard error of the median.
(E) Box plots illustrating the distribution of the model parameters m (maximum p21 production rate), θ (activation threshold) and δ (degradation rate) for the four different cellular subgroups shown in Fig. 3B-E. Black lines indicate medians of distributions; boxes include data between the 25th and 75th percentiles; whiskers extend to maximum values within 1.5× the interquartile range; outliers are displayed as black dots, far outliers as grey dots.
(F) Schematic representation of the model with no p21 production during S-phase.
(G) For the model with no p21 production during S phase, comparison of simulated (purple) and measured (magenta) p21 protein levels. Left panels display protein dynamics in single cells, right panels medians for multiple cells with the same cell cycle characteristics. The number of cells analyzed in each category is indicated. Black dashed lines indicate time of irradiation (5Gy), blue dashed lines cell divisions. Shaded regions represent the standard error of the median.
(H) Fit quality of both models for cells damaged in or progressing to S-phase. The deviation of data and model was quantified as $\chi^2 = \sum_i |data(i) - model(i)|^2$ for each fit to a single cell trajectory. Histograms of the corresponding χ^2 values are shown, with lower values indicating better fits.
(I) Comparison of the different models at the G1-S boundary of the single cell from Fig. 3D.
(J) Illustration of the function $D_S(t)$, which was used to implement a gradual increase of the p21 degradation rate upon S-phase entry.
(K) For the model with a gradual increase of the degradation rate upon S-phase entry, comparison of the simulation result and the median p21 level of cells that were irradiated in G1 and progressed to S phase.
(L) Box plots of the χ^2 distribution around the G1-S transition showing an improvement of the fit quality by gradually increasing the degradation rate. Here, $\chi^2 = \sum_{i=10\mathrm{h}}^{15\mathrm{h}} |data(i) - model(i)|^2$ was only evaluated for data points i that lie between 10 and 15 hours after the irradiation. The medians of the distributions are indicated over the boxes.

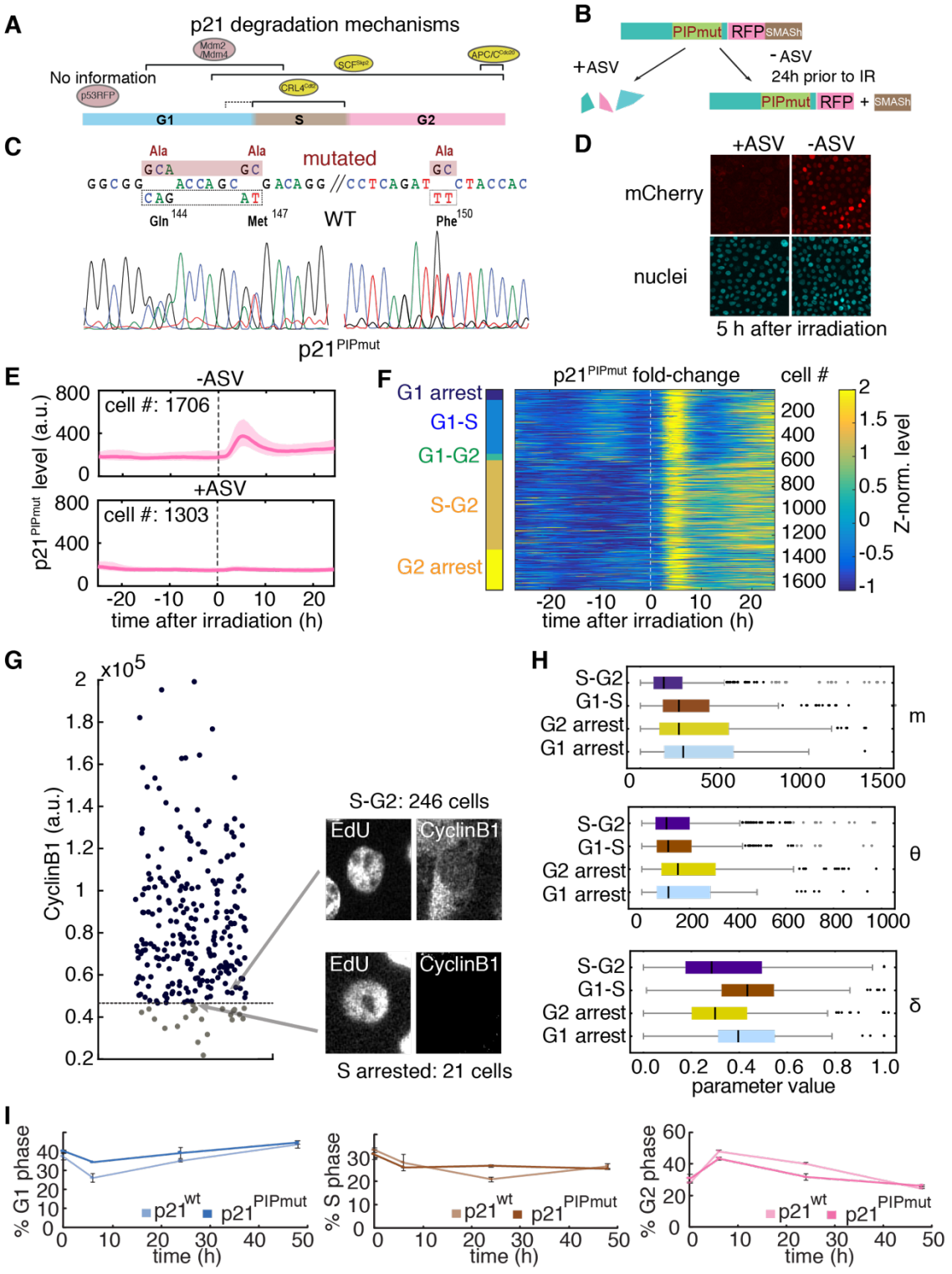

Figure S6. PCNA-mediated p21 degradation determines delayed p21 degradation during S-phase, related to Figure 3I-K and 4

(A) Potential degradation mechanisms may influence p21 stability during different cell cycle stages.

(B) Schematic illustration of a drug controllable system to degrade $p21^{PIPmut}$ in engineered cells to allow normal growth. A Small molecule–assisted shutoff (SMASh) tag was appended on C-terminus of mCherry. Under normal conditions, a protease inhibitor asunaprevir (ASV, 1 μM) was added in the medium so that the protease activity of SMASh is inhibited, which allows an internal degron to degrade newly synthesized $p21^{PIPmut}$-mCherry-SMASh. During microscopy experiments, ASV was removed from medium, the internal protease component removes SMASh to allow $p21^{PIPmut}$-mCherry accumulation and degradation under control of endogenous mechanisms.

(C) A heterozygous mutant p21 ($p21^{PIPmut}$) cell line was created using CRISPR/Cas9-mediated genome engineering. Fluorograms of the corresponding genomic regions demonstrate the presence of the indicated point mutations. See STAR methods for further details.
(D, E) $p21^{PIPmut}$ was successfully degraded by SMASh. $p21^{PIPmut}$ cells were subjected to 5Gy X-ray irradiation in absence or presence of 1 μM asunaprevir (ASV) and imaged for 24 hours. Selected microscopy images at 5th hour (D) and quantified p21 levels in populations of all tracked cells (E) are shown. Lines indicate median p21 levels, shaded areas the 25th to 75th percentile.
(F) Single cell dynamics of $p21^{PIPmut}$ in subgroups of different cell cycle progressions. Each line represents a single cell with color indicating Z-normalized fold-change. Cell numbers for each group are the same as in Figure 4B.
(G) A pulse labeling experiment was performed to determine cell cycle progression in $p21^{PIPmut}$ cells. $p21^{PIPmut}$ cells were imaged for 24 hours in the absence of ASV, incubated in EdU-containing medium for 30 mins, subjected to 5Gy ionizing radiation and imaged for another 24 hours, followed by fluorescence bleaching and single-cell immunofluorescence for EdU and Cyclin B1. Cyclin B1 levels for EdU-positive cells are shown, indicating that the majority of these cells progressed from S- to G2-phase during the DNA damage response (S-G2: 246 cells). Only a minor fraction showed no detectable Cyclin B1, suggesting that these cells were stalled in S-phase without further nucleotide incorporation. Dashed line indicates background levels of Cyclin B1 staining.
(H) Box plots illustrating the distribution of the model parameters m (maximum p21 production rate), θ (activation threshold) and δ (degradation rate) for the four different cellular subgroups shown in Fig. 4C. Black lines indicate medians of distributions; boxes include data between the 25th and 75th percentiles; whiskers extend to maximum values within 1.5× the interquartile range; outliers are displayed as black dots, far outliers as grey dots.
(I) Cell cycle distributions were measured by flow cytometry at the indicated time points after treatment with 5Gy ionizing radiation in wildtype and $p21^{PIPmut}$ cells. Error bars indicate standard deviation of triplicates. Results are representative for two independent experiments.